11-1-2013

Magnetic Interaction Reversal in Watermelon Nanostructured Cr-Doped Fe Nanoclusters

Maninder Kaur
University of Idaho

Qilin Dai
University of Wyoming

Mark Bowden
Pacific Northwest National Laboratory

Mark H. Engelhard
Pacific Northwest National Laboratory

Yaqiao Wu
Boise State University

See next page for additional authors

Magnetic interaction reversal in watermelon nanostructured Cr-doped Fe nanoclusters

Maninder Kaur,[1] Qilin Dai,[2] Mark Bowden,[3] Mark Engelhard,[3] Yaqiao Wu,[4,5] Jinke Tang,[2] and You Qiang[1,a)]
[1]*Department of Physics, University of Idaho, Moscow, Idaho 83844, USA*
[2]*Department of Physics and Astronomy, University of Wyoming, Laramie, Wyoming 82071, USA*
[3]*Environmental Molecular Sciences Laboratory, Pacific Northwest National Laboratory, Richland, Washington 99352, USA*
[4]*Department of Materials Science and Engineering, Boise State University, Boise, Idaho 83725, USA*
[5]*Center for Advanced Energy Studies, Idaho Falls, Idaho 83401, USA*

(Received 25 April 2013; accepted 26 October 2013; published online 13 November 2013)

Cr-doped core-shell Fe/Fe-oxide nanoclusters (NCs) were synthesized at varied atomic percentages of Cr from 0 at. % to 8 at. %. The low concentrations of Cr (<10 at. %) were selected in order to inhibit the complete conversion of the Fe-oxide shell to Cr_2O_3 and the Fe core to FeCr alloy. The magnetic interaction in Fe/Fe-oxide NCs (~25 nm) can be controlled by antiferromagnetic Cr-dopant. We report the origin of σ-FeCr phase at very low Cr concentration (2 at. %) unlike in previous studies, and the interaction reversal from dipolar to exchange interaction in watermelon-like Cr-doped core-shell NCs. © *2013 AIP Publishing LLC*.
[http://dx.doi.org/10.1063/1.4830434]

The giant magnetoresistance (GMR) effect,[1,2] where an antiferromagnetic (AFM) exchange coupling exists between two ferromagnetic (FM) layers separated by a certain type of magnetic or non-magnetic spacer,[3] has significant potential for application in the magnetic recording industry. Soon after the discovery of the GMR, the magnetic properties of multilayer systems (FeCr) became a subject of intensive study. The application of bulk iron-chromium (Fe-Cr) alloys has been of great interest, as these alloys exhibit favorable properties including corrosion resistance, high strength, hardness, low oxidation rate, and strength retention at elevated temperature. However, the structural and magnetic properties of Cr-doped Fe nanoclusters (NCs) have not been investigated in-depth.

Of all NCs, Fe-based clusters have unique magnetic properties as well as favorable catalytic characteristics in reactivity, selectivity, and durability.[4] The incorporation of dopant of varied type and concentration in Fe can modify its chemical ordering, thereby optimizing its electrical, optical, and magnetic properties and opening up many new applications. The substitution of an Fe atom (1.24 Å) by a Cr atom (1.25 Å) can easily modify the magnetic properties, since (i) the curie temperature (T_c) of Fe is 1043 K, while Cr is an itinerant AFM with a bulk Neel temperature $T_N = 311$ K, and (ii) Fe and Cr share the same crystal structure (bcc) with only 0.5% difference between their lattice constants.

In bulk, the mixture of Fe and Cr results in the formation of different phases of FeCr with very significant temperature dependence. As reported by Sumiyama *et al.*[5] and Cieslak *et al.*,[6] the composition range for the formation of mixed phase (bcc-Fe + σ-FeCr) in thin film is greater than 30 at. % and 35 at. % of Cr, respectively. Very few works have been published on Cr-doped NCs compared to thin films. In the NC samples, studied by Petrov *et al.*,[7] very weak lines of σ-phase appeared only when Cr content exceeded the value of 23.4 at. %. On the other hand, significant bcc α-FeCr phase formation at low Cr concentration (Cr < 13.6 at. %) was detected by Gich *et al.*[8] and Racka *et al.*[9] In our study, we observed that the σ-phase formation begins at 2 at. % of Cr in core-shell iron/iron-oxide (Fe/Fe-oxide) NCs synthesized by cluster deposition method. In particular, we observed a drastic transformation from dipolar interaction to exchange interaction at 8 at. % of Cr.

Fe/Fe-oxide core-shell NCs with variable Cr-dopant (0 at. %–8 at. %) were synthesized using a nanocluster deposition system: a combination of magnetron sputtering and gas aggregation technique. The deposition method is described in detail in our previous papers.[10–14] Cr-dopant was added at three nominal concentrations: 2 at. %, 5 at. %, and 8 at. %. Its concentration was controlled by adjusting the relative surface area of Fe and Cr within the sputtering area of the target. Four low concentrations (0, 2, 5, 8 at. %) of Cr were used to prepare Fe0%Cr, Fe2%Cr, Fe5%Cr, and Fe8%Cr samples. Five samples of each doping concentration were prepared, all of which had constant NC film thickness of ~1 μm. The concentrations of Cr were kept lower than 10 at. %, because higher Cr concentrations cause complete alteration of the metal core to FeCr alloy and the Fe-oxide shell to Cr_2O_3.

X-ray diffraction (XRD) patterns of the four NCs samples (Fig. 1(a)) show the presence of two different phases: metallic α-Fe phase, and an oxide with inverse spinel structure that can be identified as Fe_3O_4 and/or γ-Fe_2O_3. Observation of severe peak broadening indicates that the oxide-shell is composed of ultrathin crystallites with dimensions in the range 2–3 nm. The peak broadening increases with Cr concentration, while Fe5%Cr and Fe8%Cr samples indicate some extra shoulder peaks along the metallic Fe (110) peak.

An average crystallite size of NC samples obtained using the Scherrer formula falls in the range of ~25 nm, with

a)Author to whom correspondence should be addressed. Electronic mail: youqiang@uidaho.edu.

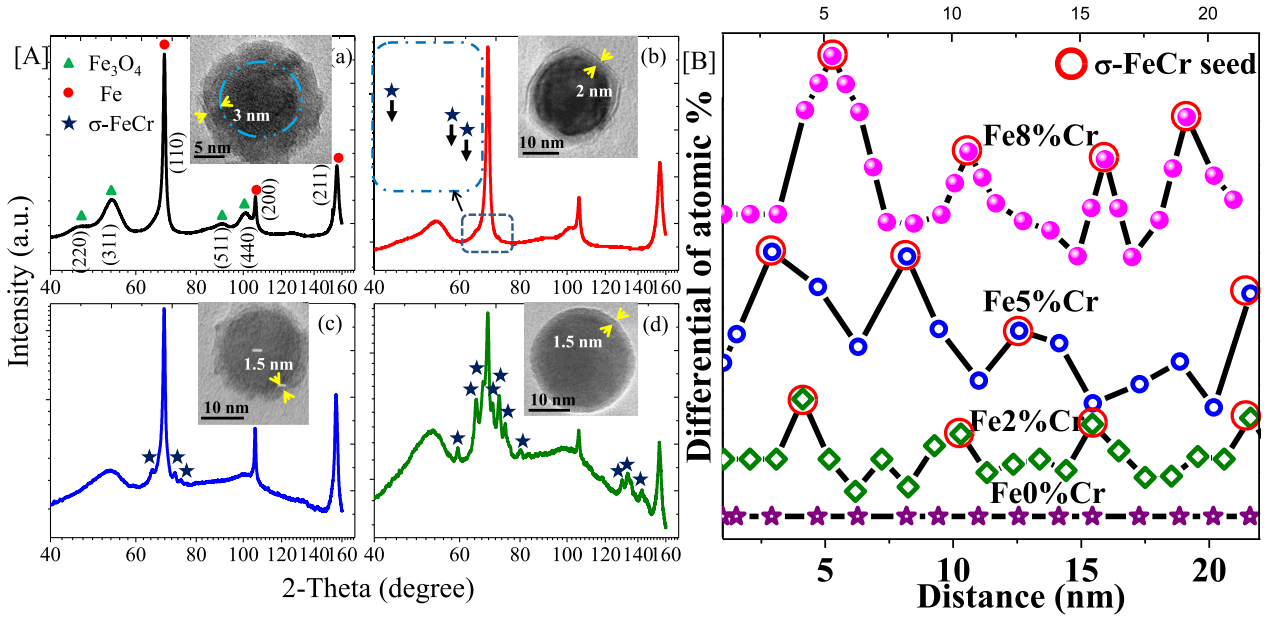

FIG. 1. (A) XRD patterns and TEM images of (a) Fe0%Cr, (b) Fe2%Cr, (c) Fe5%Cr, and (d) Fe8%Cr NCs samples. The inset figure (b) indicates the weak features of σ-FeCr phase. (B) The variation of Cr concentration in terms of differential of atomic percentage (%) measured using EDS linescan from rim to center of the cluster (shown with yellow line in TEM image) for all the samples.

small variation. The lattice parameters were derived from least squares fitting of diffraction peaks, including the (hkl) peak near 2-theta where the relative precision is much greater. It is observed that the unit cell volumes are enlarged by 0.208% (Fe2%Cr), 0.424% (Fe5%Cr), and 0.629% (Fe8%Cr) as compared to α-Fe (Fe0%Cr), and Fe (211) peak shifts toward lower angle with Cr concentration. Our data are statistically significant with respect to previously published data.[7] The unaltered lattice parameter of Fe-oxide ($\sim$8.399 Å) indicates that most of the Cr remains in the metal phase.

The extra novel peaks of Fe5%Cr and Fe8%Cr were recognized to indicate FeCr intermetallic phase; it is present in Fe2%Cr, but the corresponding features are very weak due to strong intensity from the Fe (110) plane. These features become stronger with Cr concentration. It is assumed that the cell is distorted slightly with Cr dopant because of the core-shell microstructure, and it eventually forms another phase, the σ (Fe,Cr) phase.[15] Neither pure Cr nor corundum structured Cr_2O_3 was observed in the XRD patterns. Hence the Cr-doped NCs consist of mixed phases containing both α-Fe and σ-FeCr.

The inset of Fig. 1(a) shows high resolution transmission electron microscope (HRTEM) overviews of all NC samples. A NC crystal axis oriented along the electron beam direction shows two contrasts: a dark core corresponding to α-Fe and a light-grey shell structure of the spinel phase of oxide (γ-Fe_2O_3 and/or Fe_3O_4). Detailed morphology, electronic structure, and crystalline structure of core-shell Fe/Fe-oxide NCs have been reported by our group in several publications.[16–18] The quantitative analysis of TEM-energy dispersive spectroscopy (EDS) indicates that the Fe:Cr atomic ratio consistently falls to 97:3 for Fe2%Cr, 95:5 for Fe5%Cr, and 93:9 for Fe8%Cr samples (Fig. 1(b)). The EDS line-scan from rim to center of each cluster shows that the Cr concentration increases from the outer rim to the phase boundary and then varies relative to the different grains (Fe or FeCr) present in the core. This result indicates that the core is made up of both bcc-Fe and σ-FeCr. Here, the depth profile is normalized as Fe + Cr = 100%. The differential of atomic percentage of Cr-doped samples shows the alternative peaks of Cr (marked by circle), which elucidate the distribution of FeCr seeds in the α-Fe core.

Since a small percentage of Cr is distributed on the sample surface, the exposure of NCs to O_2 atmosphere (2 sccm) in the deposition chamber does lead to the preferential oxidation of Cr, forming Cr_2O_3, as detected by X-ray photoelectron spectroscopy (XPS) analysis with Cr $2p_{3/2}$line at 576.6 eV. Given the fact that XPS is a surface sensitive tool, Cr_2O_3 is present only on the NC surface. It is a well-known phenomenon that the oxidation resistance of a superalloy relies on preferential oxidation of Cr to form a Cr_2O_3 layer, which prevents the oxidation of the underlying metal.[19] In our case, the presence of min Cr_2O_3 on the NC surface (oxide-shell) inhibits further oxidation of the cluster; hence, the shell thickness decreases with Cr concentration (2.5 nm (Fe0%Cr), 2.0 nm (Fe2%Cr), 1.5 nm (Fe5%Cr), 1.5 nm (Fe8%Cr)), as confirmed by XRD and TEM.

Saturation magnetization (M_s), coercive field (H_c), and exchange bias field (H_E) of all samples increase with reducing temperature when the samples were field cooled (20 kOe) from 300 K to 5 K. The following three observations were extracted from the *M-H* curves ($\pm$50 kOe) as the Cr dopant increases: (i) M_s decreases, (ii) H_E and H_c increase, and (iii) the hysteresis curve shrinks near the zero field axis.

The dopant atom, Cr ($4s^1\ 3d^5$), with its smaller number of valence electrons, couples antiferromagnetically to the Fe ($4s^2\ 3d^6$) atom. The antiparallel alignment of Cr spin to Fe spin is also observed between Fe and Cr layers.[20] The AFM spin coupling between Fe and Cr in σ-FeCr leads to a decrease of M_s from 132 emu/g (Fe0%Cr) to 75 emu/g (Fe8%Cr) measured at 5 K.

TABLE I. The cluster size determined from TEM; and the coercive field, exchange bias field and % shrink of hysteresis curve measured for all samples at 5 K.

	TEM (nm)	T = 5 K		
Sample	Mean size	H_c (Oe)	H_E (Oe)	%S
Fe0%Cr	24 ± 0.07	793	119	0.0131
Fe2%Cr	25 ± 0.08	964	185	0.0128
Fe5%Cr	23 ± 0.10	1156	227	0.0108
Fe8%Cr	24 ± 0.08	1293	253	0.0086

A small amount of AFM Cr_2O_3 ($T_N = 307$ K),[21] which is present with other oxides (Fe_3O_4 and γ-Fe_2O_3) in the oxide-shell enhances the net H_E and might cause the *M-H* curve to shrink near the zero field axis in Cr-doped samples. Exchange bias is a coupling phenomenon at magnetic interfaces (Fe and Fe-oxides) which manifests itself most prominently in the shift of the hysteresis curve along the magnetic-field axis and is quantified by the magnitude (H_E) of that shift. In Cr-doped samples, H_E increases with the Cr concentration (Table I). The increase of H_E from 119 Oe (Fe0%Cr) to 253 Oe (Fe8%Cr) and H_c from 793 Oe (Fe0%Cr) to 1293 Oe (Fe8%Cr) is ascribed to variation of anisotropy due to incorporation of AFM Cr_2O_3 in the shell (detected by XPS). It is hypothesized that the Cr present on the outer surface of a NC oxidizes to Cr_2O_3 during the formation of the oxide-shell[8,9] and effectively contributes to the net anisotropy. The irreversibility field[22] (H_{irr}), where two curves of the hysteresis loop close, measures higher for Fe8%Cr ($H_{irr}(5\,K) \sim 8.5$ kOe) than for Fe0%Cr ($H_{irr}(5\,K) \sim 5.5$ kOe). The higher value of H_{irr} confirms the presence of unsaturated, highly anisotropic component (Cr_2O_3) in Cr-doped samples.

Figure 2(a) shows the shrinking of the hysteresis curve near the zero-field axis as the Cr concentration increases from 0 at. % to 8 at. %. The curves are measured up to ±50 kOe, but it is shown for ±10 kOe in order to make the area around zero-field axis more noticeable. How much the curve shrinks is measured as $\%\,S = H_a/H_b$ (Table I), where H_a and H_b are the widths of the loop measured at the zero-field axis and at remanent magnetization, respectively.

The undoped NC system consists of α-Fe and Fe-oxides, and shows symmetric hysteresis with bias effect. As Cr is doped into the NC system, the tight-waist of the hysteresis curve appears. Hence the observed anomaly is linked to the additional phases that arise with the incorporation of Cr into this Fe/Fe-oxide NC system, which is recognized to be σ-FeCr (core) and Cr_2O_3 (shell). Therefore, the tight waist of the curve originates either from σ-FeCr and/or AFM Cr_2O_3.

Compared to pure α-Fe core in Fe0%Cr, Cr-doped samples consist of a mixture of α-Fe and σ-FeCr. The paramagnetic behavior of the σ-phase could be the cause of shrink in the hysteresis curve, because the observed anomaly is temperature dependent and disappears at high temperature.

Considering the rotation of oxide-spins relative to core-spins presents another possible explanation. In the core-shell system, the FM core-spins easily rotate with the applied field's direction as compared to surface (frozen)/interface (pinned) spins, which require extra energy to reorient. The oxide-shell of doped samples consists of a mixture of AFM Cr_2O_3 and ferrimagnetic (FI) Fe-oxides. Within a cluster, the oxide-spins (AFM and FI) interact with each other as well as with FM Fe-spins through an interface. A microscopic view of spin configurations in the core-shell NC is shown in the inset of Fig. 2(a). The interactions between the three different magnetic phases (AFM, FI, and FM) increase the net anisotropy and result in the increase of both H_c and H_E (Table I). Since AFM interaction is stronger than FI, the sample's surface/interface spins (AFM and FI) require additional energy after field-cooling compared to the unfrozen, original FI-spins to switch from a positive to a negative field. In other words, the surface/interface spins resist orientation after switching the field direction. As the surface spins reverse in the lower field, the core-spins rapidly rotate along with them. Once the sample is saturated along the negative field axis, it surmounts the same energy barrier to saturate along the positive axis to complete the hysteresis curve. The large difference between the fields required to reverse the

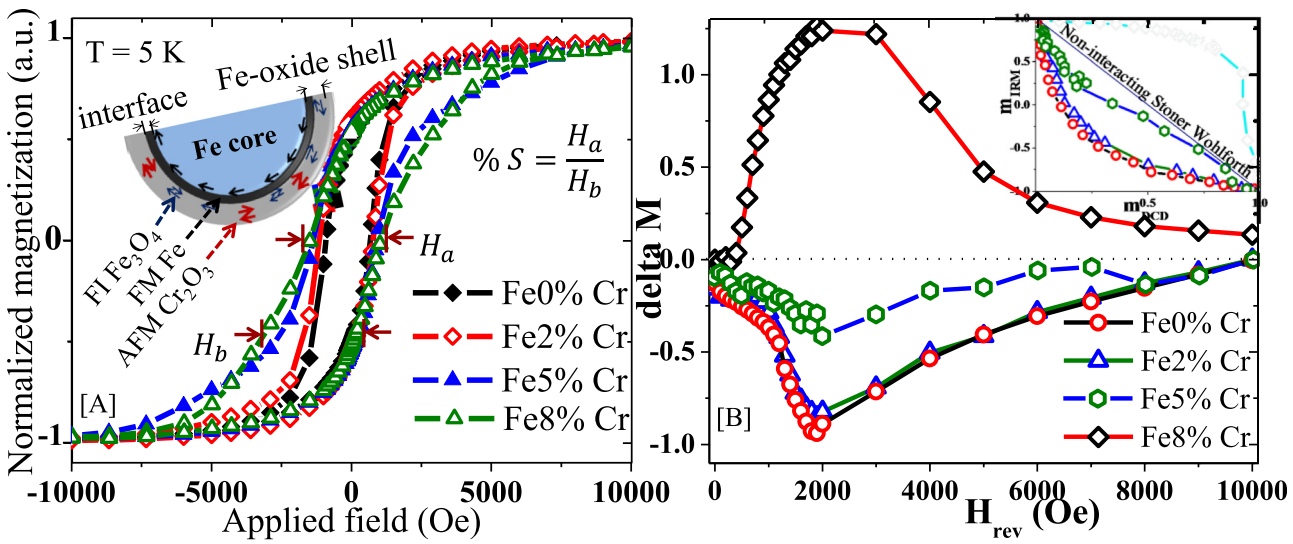

FIG. 2. (A) Hysteresis curves of undoped and Cr-doped Fe NCs. The inset figure represents the micromagnetic view of spin configurations in core-shell nanostructure. (B) Delta M plot for all samples at 5 K. The inset figure represents the Henkel plot.

core-spins in comparison with the shell-spins causes the curve to appear tight-waisted near the field axis.

Though the AC demagnetized state is not considered to be a statistically random state, the DC demagnetized state is considered to be a random state and is comparable with the microscopically and randomly demagnetized states.[23,24] In the present case, the DC-demagnetized state has been studied. Isothermal remanent magnetization (IRM) and DC-demagnetization remanence (DCD) curves are used to study the interactions between the clusters. These curves describe the field dependence of the remanence; they were measured as a function of applied field up to ±50 kOe for two different temperatures (5 K and 300 K). $m_{DCD}(H)$ and $m_{IRM}(H)$ are the reduced terms with remanence saturation value for DCD and IRM curves. A mean interaction field (H_{int})[25] value of −375 Oe was obtained from the field derivative of m_{IRM} and m_{DCD} curves for Fe0%Cr. The value decreased for 2 at. % (−357 Oe) and 5 at. % (−47 Oe), and then increased and switched its sign for 8 at. % of Cr (+2689 Oe). This implies that the increase of Cr concentration (0–8 at. %) in the NC system makes the dipolar interaction weaker and exchange interaction stronger. The presented result is supported by the Henkel plot,[26] $m_{IRM}(H)$ versus $m_{DCD}(H)$, and the delta M (ΔM) plot,[27] ΔM value versus reversible field (H_{rev}); both plots are illustrated in Fig. 2(b). The straight solid-line (Henkel plot) is the theoretical Wohlfarth equation[12] for non-interacting systems. The Henkel plots of Fe0%Cr, Fe2%Cr, and Fe5%Cr lie below this solid-line, indicating the dipolar (demagnetizing) interaction, while the curve above the line for Fe8%Cr indicates the exchange interaction.

The complex mixing of interactions (dipolar and exchange) results in negative ΔM values $(\Delta M < 0)$ in core-shell NC systems (0–5 at. %) that indicate the systems' demagnetized state.[28,29] On the other hand, a positive ΔM value $(\Delta M > 0)$ favoring the exchange interaction is observed in Fe8%Cr. At room temperature, the ΔM values are negative for all samples. This demagnetized state under unblocked regime decreases with Cr content but does not show much deviation from the undoped NC system.

The origin of exchange interaction in the core with the inclusion of Cr in the core-shell Fe NC is explained by considering the core-shell energy model, which is modified for the Cr-doped NC. The total energy of NC assembly is written as

$$E_T = g\sum_{i,j}\frac{(\hat{S}_i\cdot\hat{S}_j)-3(\hat{S}_i\cdot\hat{R}_{ij})(\hat{S}_j\cdot\hat{R}_{ij})}{R_{ij}^3} - J^{interface}\sum_{\langle i,j\rangle}(\hat{S}_i\cdot\hat{S}_j) - J^{core}\sum_{\langle i,j\rangle}(\hat{S}_i\cdot\hat{S}_j) - K_{core}\sum_i(\hat{S}_i\cdot\hat{e}_i)^2 - K_{shell}\sum_i(\hat{S}_i\cdot\hat{e}_i)^2 - h\sum_i(\hat{S}_i\cdot\hat{H}),$$

where $\hat{S}_i$ is the magnetic moment direction of NC i, $\hat{e}_i$ is easy axis direction, and $\hat{R}_{ij}$ is the center-to-center cluster distance. J^{core} is the exchange constant between core spins and $J^{interface}$ is counterpart to core-shell spins. K_{core} and K_{shell} are the core and surface anisotropy constants. The above equation represents two exchange energy terms: one for the interface interaction between the core and shell spins and another for the core interaction between the FeCr and Fe spins. Here, the magnitudes of the dipolar and exchange energies are much greater than other energies. The sum of the dipole energy (E_d), with dipole coupling constant g, and the Zeeman energy (E_z), where $h(=M_sVH)$ favors the dipolar interaction; in the absence of Cr that dominates the exchange energy and hence favors the net dipolar interaction in Fe0%Cr. Similar behavior was also reported by Bianco *et al.* in Fe/Fe-oxide granular system.[30]

With the inclusion of Cr in a core-shell system, σ-FeCr originates as an intermetallic phase with bcc-Fe. The structural model of a doped core-shell NC looks like a watermelon as shown in Fig. 3. The seeds of melon act like σ-phase, spreading uniformly throughout the core (Fe pulp). The grains of σ-FeCr and bcc-Fe are exchange coupled across their grain boundaries. Hence, there are two places in a NC where the exchange interaction occurs: (i) at the interface between the core and shell and (ii) in the core between the seed (FeCr) and pulp (Fe).

The dipolar and exchange interactions are the primary interactions present in Fe/Fe-oxide core-shell NC system. As compared to other Cr-doped NC samples, the undoped NC (Fe0%Cr) exhibits higher dipolar interactions due to the higher magnetization (132 emu/g). Since the dipolar interaction was much stronger than the exchange interaction, the Henkel plot falls on the negative side of the Wohlfarth line, returning a negative ΔM value. The dipolar interaction decreases with the concentration of Cr and therefore the magnitude of ΔM decreases for Fe2%Cr $(\Delta M = -0.85)$ and Fe5%Cr $(\Delta M = -0.41)$ as compared to Fe0%Cr $(\Delta M = -1.01)$. It shows that the two types of interactions compete strongly with each other as the magnitude of exchange energy evolves. The extra exchange energy comes from the exchange interaction that arises between the grains of σ-FeCr and bcc-Fe after Cr is doped into the NC. The number of σ-FeCr seeds increases with Cr concentration, which further enhances the exchange energy.

Competition between the interactions brings the ΔM value closer to zero and towards positive values while the Henkel plot approaches the non-interaction line. The strength of both interactions appears nearly comparable for Fe5%Cr. As the contribution of exchange energy becomes higher than dipolar energy, both of the interactions compensate each other and cross over the Wohlfarth line. It is observed that for Fe8%Cr, when the strength of exchange interaction

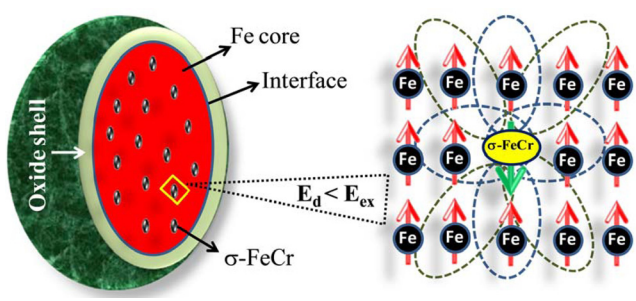

FIG. 3. Watermelon model of Cr-doped core-shell NC. The σ-FeCr grain acts like melon seed which is exchange coupled with the surrounded bcc-Fe (pulp).

overcomes the dipolar, the ΔM (+1.23) value is positive and the Henkel plot is on the right side of the Wohlfarth line. The significant contribution of interaction switching comes from the exchange interaction between the σ-FeCr and bcc-Fe, because the interface interaction can't stand alone to compete with the dipolar interaction. Strong exchange coupling in the core has a higher contribution to the overall interactions than the interparticle dipolar interactions, especially in the Fe8%Cr. In this way, the magnetic interaction in Fe core-shell NC system can be controlled by varying the doping concentration of Cr. The femtosecond switching from AFM to FM[31] in $Pr_{0.7}Ca_{0.3}MnO_3$ opens a new door to Cr-doped Fe core-shell like nanostructured system for use in the magnetic recording industry because smaller size and faster switching speed are essential to the field's continued advancement.

In summary, we have demonstrated the formation of σ-FeCr phase with bcc-Fe at very low concentration of Cr (2 at. %) in core-shell Fe NCs. The decrease of shell thickness and increase of exchange bias field were caused by the formation of Cr_2O_3 within the Fe-oxide shell. The exchange interaction competed with the dipolar interaction upon inclusion of Cr-dopant, which results in watermelon like core-shell NCs and interaction reversal in 8 at. % of Cr.

This study was supported by U.S. Department of Energy (DOE) under Contracts (DE-FC07-08ID14926) and DOE INL-CAES LDRD (DE-AC07-05ID14517). Parts of the work were conducted in the William R. Wiley Environmental Molecular Sciences Laboratory (EMSL), a DOE User Facility operated by Battelle for the DOE Office of Biological and Environmental Research. Pacific Northwest National Laboratory is operated for the DOE by Battelle under Contract DE-AC05-76RL01830.

[1]M. N. Baibich, J. M. Broto, A. Fert, F. N. Van Dau, and F. Petroff, Phys. Rev. Lett. **61**, 2472 (1988).
[2]G. Binasch, P. Grünberg, F. Saurenbach, and W. Zinn, Phys. Rev. B **39**, 4828 (1989).
[3]P. Grünberg, R. Schreiber, Y. Pang, M. B. Brodsky, and H. Sowers, Phys. Rev. Lett. **57**, 2442 (1986).
[4]C. Zhenhua, Y. Hongge, K. Zhitao, S. Yi, and H. Peiyun, Trans. Nonferrous Met. Soc. China **11**(5), 725 (2001).
[5]K. Sumiyama, N. Ohshima, and Y. Nakamura, Trans. Jpn. Inst. Met. **28**, 699 (1987).
[6]J. Cieślak, B. F. O. Costa, S. M. Dubiel, M. Reissner, and W. Steiner, J. Phys. Condens. Matter **17**, 2985 (2005).
[7]Y. I. Petrov, E. A. Shafranovsky, Y. F. Krupyanskii, and S. V. Essine, J. Appl. Phys. **91**, 352 (2002).
[8]M. Gich, E. A. Shafranovsky, A. Roig, A. Ślawska-Waniewska, K. Racka, L. Casas, Y. I. Petrov, E. Molins, and M. F. Thomas, J. Appl. Phys. **98**, 024303 (2005).
[9]K. Racka, A. Ślawska-Waniewska, A. Krzyżewski, M. Gich, A. Roig, E. A. Shafranovsky, and Y. I. Petrov, J. Magn. Magn. Mater. **320**, e683 (2008).
[10]S. Kwon, Y. Jeong, and S. Jeong, J. Nanosci. Nanotechnol. **6**, 3647 (2006).
[11]Y. Qiang, J. Antony, A. Sharma, J. Nutting, D. Sikes, and D. Meyer, J. Nanopart. Res. **8**, 489 (2006).
[12]M. Kaur, J. S. McCloy, W. Jiang, Q. Yao, and Y. Qiang, J. Phys. Chem. C **116**, 12875 (2012).
[13]Y. Qiang, J. Antony, M. G. Marino, and S. Pendyala, IEEE Trans. Magn. **40**, 3538 (2004).
[14]C. Wang, D. Baer, J. Amonette, M. Engelhard, J. Antony, and Y. Qiang, Microsc. Microanal. **13**, 1054 (2007).
[15]S. Oda and M. Ohkoshi, IEEE Trans. J. Magn. Jpn. **2**, 1005 (1987).
[16]C. M. Wang, D. R. Baer, L. E. Thomas, J. E. Amonette, J. Antony, Y. Qiang, and G. Duscher, J. Appl. Phys. **98**, 094308 (2005).
[17]C. Wang, D. R. Baer, J. E. Amonette, M. H. Engelhard, J. Antony, and Y. Qiang, J. Am. Chem. Soc. **131**, 8824 (2009).
[18]C. M. Wang, D. R. Baer, J. E. Amonette, M. H. Engelhard, Y. Qiang, and J. Antony, Nanotechnology **18**, 255603 (2007).
[19]P. Y. Hou and J. Stringer, Oxidation of Metals **34**, 299 (1990).
[20]W. Gong, H. Li, Z. Zhao, G. C. Hadjipanayis, V. P. Papaefthymiou, A. Kostikas, and A. Simopouos, J. Appl. Phys. **70**, 5900 (1991).
[21]Y. Chen, K. Ding, L. Yang, B. Xie, F. Song, J. Wan, G. Wang, and M. Han, Appl. Phys. Lett. **92**, 173112 (2008).
[22]D. Fiorani, L. D. Bianco, A. M. Testa, and K. N. Trohidou, J. Phys. Condens. Matter **19**, 225007 (2007).
[23]R. D. McMichael, F. Vajda, and E. Della Torre, J. Appl. Phys. **75**, 5692 (1994).
[24]P. D. Mitchler, R. M. Roshko, and E. D. Dahlberg, IEEE Trans. Magn. **34**, 1282 (1998).
[25]X. Batlle, M. García del Muro, and A. Labarta, Phys. Rev. B **55**, 6440 (1997).
[26]O. Henkel, Phys. Status Solidi B **7**, 919 (1964).
[27]T. Thomson, K. O'Grady, and G. Bayreuther, J. Phys. Appl. Phys. **30**, 1577 (1997).
[28]N. Powers, M. L. Yan, L. Gao, S. H. Liou, and D. J. Sellmyer, J. Appl. Phys. **91**, 8641 (2002).
[29]N. Lakshmi, H. Bhargava, O. P. Suwalka, K. Venugopalan, V. Sebastian, V. R. Reddy, and A. Gupta, Phys. Rev. B **80**, 174425 (2009).
[30]L. Del Bianco, A. Hernando, and D. Fiorani, ChemInform **36**, 217–238 (2005).
[31]T. Li, A. Patz, L. Mouchliadis, J. Yan, T. A. Lograsso, I. E. Perakis, and J. Wang, Nature **496**, 69 (2013).